RSC Advances

PAPER

View Article Online
View Journal | View Issue

Cite this: *RSC Adv.*, 2020, **10**, 32845

MIL-101(Cr)–cobalt ferrite magnetic nanocomposite: synthesis, characterization and applications for the sonocatalytic degradation of organic dye pollutants†

Abbasali Mokhtari Andani,[a] Tayebeh Tabatabaie,*[a] Saeed Farhadi *[b] and Bahman Ramavandi [c]

In this study, for the first time, a novel magnetically recyclable MIL-101(Cr)/$CoFe_2O_4$ nanocomposite was prepared *via* a facile solvothermal method. The morphology, structural, magnetic and optical properties of the nanocomposite were characterized *via* field emission scanning electron microscopy (FE-SEM), transmission electron microscope (TEM), energy dispersive X-ray (EDX) spectroscopy, X-ray diffraction (XRD), Fourier transform infrared spectroscopy (FT-IR), vibrating sample magnetometer (VSM), UV-visible spectroscopy (UV-visible) and BET surface area analysis. Furthermore, the sonocatalytic activity of the MIL-101(Cr)-based magnetic nanocomposite was explored for the degradation of organic dye pollutants such as Rhodamine B (RhB) and methyl orange (MO) under ultrasound irradiation in the presence of H_2O_2. Under optimized conditions, the degradation efficiency reached 96% for RhB and 88% for MO. The sonocatalytic activity of MIL-101(Cr)/$CoFe_2O_4$ was almost 12 and 4 times higher than that of the raw MIL-101(Cr) and pure $CoFe_2O_4$, respectively. The improved sonocatalytic performance of the as-prepared binary nanocomposite can be attributed to the relatively high specific surface area of MIL-101(Cr) and magnetic property of $CoFe_2O_4$, as well as the fast generation and separation of charge carriers (electrons and holes) in MIL-101(Cr) and $CoFe_2O_4$. In addition, the trapping tests demonstrated that ·OH radicals are the main active species in the dye degradation process. Moreover, the most influencing factors on the sonocatalytic activity such as the H_2O_2 amount, initial dye concentration and catalyst dosage were investigated. Finally, the nanocomposite was magnetically separated and reused without any observable change in its structure and performance even after four consecutive runs.

Received 4th June 2020
Accepted 14th August 2020

DOI: 10.1039/d0ra04945j

rsc.li/rsc-advances

1. Introduction

Nowadays, considerable attention is being paid to the veritable color contamination issues. Dyes are widely utilized in various industries including the paint, fashion, printing, coloring, materials and other production industries, which can significantly cause water contamination when untreated wastewater is discharged into the environment due to their non-biodegradable, exceptionally poisonous, cancer-causing and mutagenic properties.[1–4] Thus, currently, various strategies including advanced chemical oxidation (AOP), ion exchange, organic treatment and adsorption have been developed and utilized for the remediation of dyes in wastewater.[1,5–11] Among the AOP techniques, sonolysis has been widely used to degrade organic pollutants. The chemical effect of ultrasound (US) comes from acoustic cavitation, which leads to the formation of bubbles that develop and collapse in the liquid. The collapse of bubbles in solution results in the generation of spots with high localized temperature and pressure. Under these extraordinary conditions, water molecules are broken, producing highly reactive hydroxyl radicals, which attack and oxidize the organic dyes in water.[12,13] However, the US alone is not efficient for the degradation of target organic pollutants because of the long time and high amount of energy required for considerable degradation. Thus, to overcome this issue, sonocatalysts (catalysts active under ultrasonic irradiation) can be utilized in aqueous solutions for the degradation of organic pollutants. The presence of the insoluble sonocatalysts in the reactive solution accelerates the generation of ·OH under ultrasonic irradiation.[14,15] In previous reports, different semiconductors such as Cu_2S,[1] ZnO–biosilica,[16] $KNbO_3$,[17] $LuFeO_3$,[18] Fe_3O_4–graphene/ZnO@SiO_2 (ref. 19) and La-doped ZnO[20] have been

[a]Department of Environment, Bushehr Branch, Islamic Azad University, Bushehr, Iran. E-mail: Tabatabaie20@yahoo.com; Fax: +98 77 33550640; Tel: +98 77 33552501

[b]Department of Chemistry, Lorestan University, Khoramabad 68151-433, Iran. E-mail: farhadi.s@lu.ac.ir; Fax: +98 66 33120618; Tel: +98 66 33120611

[c]Department of Environmental Health Engineering, Faculty of Health and Nutrition, Bushehr University of Medical Sciences, Bushehr, Iran

† Electronic supplementary information (ESI) available. See DOI: 10.1039/d0ra04945j

studied for their sonocatalytic activity and utilized as sonocatalysts. However, their separation and reuse are still a challenge. Therefore, it is necessary to develop new magnetic sonocatalysts with high catalytic activity that can be easily recycled.

Nano/micrometer-scale spinel-type ferrites (MFe_2O_4; M = Ni, Fe, Co, and Cu) have exhibited extraordinary potential for numerous applications such as the removal of pollutants, medical diagnostics and drug delivery.[21] Among them, cobalt ferrite ($CoFe_2O_4$) has been widely studied as a magnetic material and photocatalyst because of its magnetism, high thermal stability, electronic conductivity, and noteworthy catalytic capability.[22,23] These properties made it a suitable candidate for us to investigate its capability as a sonocatalyst. The probable sonocatalytic degradation mechanism is based on both light and the "hot spots" derived from the ultrasonic cavitation effect. Firstly, it is well known that the sonoluminescence caused by the ultrasonic cavitation effect can generally generate lights with a wide wavelength range.[24,25] The generated light with an appropriate wavelength can excite the applied nanoparticles in the solution, acting as a sonocatalyst to perform pollutant degradation. Secondly, as is known, the "hot spots" produced by the ultrasonic cavitation effect in aqueous medium can achieve very high temperatures (more than 1000 °C). These high temperatures are sufficient to break down some H_2O molecules on the surface of the catalyst and produce hydroxyl radicals (·OH). These heat energies of the "hot spots" can also excite the prepared nanoparticles similar to light.[24,25] Under the excitation of the generated light and heat, electrons migrate from the valence band (VB) to the conduction band (CB) of the nanoparticles, resulting in the formation of e^-/h^+ pairs in the inner or on the surface of the nanoparticles. However, $CoFe_2O_4$ has serious drawbacks including the easy recombination of e^-/h^+ pairs and high agglomeration in solution, which decrease its catalytic activity. Thus, it is conceivable to couple $CoFe_2O_4$ nanoparticles with other semiconductors such as porous materials with a high surface area, overcoming the above-mentioned problems and upgrading their catalytic performance.

Metal organic frameworks (MOFs) are hybrid crystalline porous materials with structures consisting of a regular array of positively charged metal ions or metallic clusters associated with bi- or multipodal organic linkers.[26] Currently, MOFs have experienced rapid development due to their versatile applications such as catalysis, storage and separation. Recent research has shown that these semiconducting materials are absolutely effective as catalysts for the photocatalytic degradation of organic pollutants.[27] Among the different MOFs, MIL-101(Cr) is one of the foremost investigated and exceptionally interesting materials due to its mesoporous structure, huge surface area and great hydrothermal stability, and thus has been widely explored for the adsorption of pollutants, catalysis, photocatalysis and drug delivery.[28,29] Furthermore, these properties make MIL-101(Cr) a great candidate for sonocatalytic activity, and coupling it with narrow band-gap magnetic semiconductors (*e.g.* $CoFe_2O_4$) can be an effective way for enhancing its catalytic activity and its recyclability employing an appropriate external magnet.

In the present study, a new magnetic binary composite, namely MIL-101(Cr)/$CoFe_2O_4$, was prepared *via* a hydrothermal method and its sonocatalytic activity was studied for the degradation of Rhodamine B (RhB) and methyl orange (MO) in water as organic pollutants under US irradiation in the presence of H_2O_2 as a hydroxyl radical (·OH) source. Besides, the effects of various parameters such as initial dye concentration, sonocatalyst dosage, scavengers and H_2O_2 amount were evaluated. Moreover, the sonocatalytic activity of MIL-101(Cr)/$CoFe_2O_4$ was compared with that of pure $CoFe_2O_4$, and MIL-101(Cr) under the same conditions. To the best of our knowledge and based on the literature review, there is no report on the synthesis and application of the MIL-101(Cr)/$CoFe_2O_4$ nanocomposite as a sonocatalyst for the sonodegradation of organic dyes, particularly in the presence of H_2O_2 as an environmental-friendly oxidizing agent.

2. Experimental

2.1. Materials

Chromium nitrate nonahydrate ($Cr(NO_3)_3 \cdot 9H_2O$, 98%), cobalt nitrate hexahydrate ($Co(NO_3)_2 \cdot 6H_2O$, 98.5%), terephthalic acid (TPA, 98%), sodium hydroxide (NaOH), iron(III) nitrate nonahydrate ($Fe(NO_3)_3 \cdot 9H_2O$, 98%), dimethyl formamide (DMF, 99%), ethanol (C_2H_5OH, 96%), disodium ethylenediaminetetraacetate (Na_2EDTA, 99%), silver nitrate ($AgNO_3$, 98%), 1,4-benzoquinone (BQ, 98%), *t*-butyl alcohol (*t*-BuOH, 99%), Rhodamine B (RhB, $C_{28}H_{31}ClN_2O_3$, 98%), methyl orange (MO, $C_{14}H_{14}N_3NaO_3S$, 98%) and other chemicals were obtained from Merck Company and used as received.

2.2. Synthesis of $CoFe_2O_4$ nanoparticles

The $CoFe_2O_4$ nanoparticles were prepared *via* a hydrothermal method. $Fe(NO_3)_3 \cdot 9H_2O$ (1.71 g) and $Co(NO_3)_2 \cdot 6H_2O$ (0.62 g) were added to deionized water (25 mL) and the solution was stirred at room temperature for 1 h. Then, 1 mol L^{-1} NaOH aqueous solution was added to the suspension to adjust the pH to 11 while stirring for 1 h. The solution was then transferred to a teflon-lined autoclave bomb and kept in an oven for 12 h at 180 °C. Finally, the black product was magnetically collected and was washed with absolute ethanol and deionized water.

2.3. Synthesis of MIL-101(Cr)/$CoFe_2O_4$

The binary magnetic MIL-101(Cr)/$CoFe_2O_4$ nanocomposite was synthesized *via* a hydrothermal method. Briefly, 0.16 g of synthesized $CoFe_2O_4$ nanoparticles was added to 14 mL deionized water and sonicated for 1 h. Then, 0.5 g of TPA and 1.2 g of $Cr(NO_3)_3 \cdot 9H_2O$ were added to $CoFe_2O_4$ suspension and it was rigorously agitated for 1 h at room temperature. Afterwards, the resultant suspension was kept for 12 h at 200 °C under autogenous pressure after it was transferred to a 50 mL teflon-lined stainless steel autoclave. The obtained product was then removed from the oven and left to cool to room temperature. To obtain an extra-pure sample, the resultant mixture was consecutively flushed several times with DMF and ethanol solvents to remove any possible impurities from the unreacted

TPA on its surface. The ICP-AES results indicated that the loading amount of MIL-101(Cr) in the as-fabricated MIL-101(Cr)/$CoFe_2O_4$ nanocomposite was approximately 64.80 wt%.

2.4. Characterization methods

FT-IR spectra were recorded on a spectrophotometer (Shimadzu FT-IR 8400S, Japan) using KBr pellets in the wavelength range of 400–4000 cm^{-1}. XRD patterns of the powder samples were recorded using an X-ray diffractometer (XPertPro Panalytical, Netherland) using Ni-filtered CuKα radiation ($\lambda = 1.5406$ Å). UV-vis spectra were measured in the spectral range of 200–800 nm on a spectrophotometer (Cary 100 Conc, Varian Company, USA). A homogeneous suspension in water was formed by sonication for 40 min for the UV–vis studies of the samples. The magnetic measurements were performed utilizing a vibrating sample magnetometer (VSM, Magnetic Danesh Pajoh Kashan Co., Iran) at a maximum magnetic field of 10 kOe. The Brunauer–Emmett–Teller surface area measurement (PHS-1020, China) was performed utilizing N_2 at 77 K as the adsorbing gas. FE-SEM images were obtained using a scanning electron microscopy system (MIRA3 TESCAN, Czech Republic) coupled with a link energy-dispersive X-ray (EDX). TEM analysis was performed using a transmission electron microscope (Philips CM120, The Netherlands) at the acceleration voltage of 120 kV. In addition, an ultrasonic bath (Sonic 6MX; England) with 100 W output acoustic power and frequency of 37 kHz was utilized to investigate all the sonodecomposition reactions of dyes. Inductively coupled plasma atomic emission spectroscopy (ICP-AES, model OEC-730, USA) was utilized to identify the concentrations of Cr, Fe and Co in the filtrate.

2.5. Sonodecomposition tests

To examine the sonocatalytic decomposition of RhB as an organic cationic dye and MO as an organic anionic dye over the desired catalysts in aqueous solution, an ultrasonic device was utilized. Typically, a specific amount of magnetic MIL-101(Cr)/$CoFe_2O_4$ catalyst (0.5 g L^{-1}) was transferred to the dye aqueous solution (25 mg L^{-1}, 50 mL), and subsequently the resulting solution was stirred for 30 min in the dark. This blending step allows adsorption–desorption equilibrium to be achieved between the catalyst surface and organic dye. At that point, the solution was subjected to US irradiation in the presence of H_2O_2 (60 mmol L^{-1}). After the required interval, the reaction process was halted and 2 mL of the aqueous solution was withdrawn, followed by the separation of the MIL-101(Cr)/$CoFe_2O_4$ nanocomposite from the supernatant solution utilizing an external magnetic field, but in some cases it was centrifuged for 5 min at 5000 rpm for better separation. Finally, the residual solution of the organic dye was analyzed using a UV-vis spectrophotometer at a wavelength of 557 and 467 nm to evaluate the concentration of residual RhB and MO dyes, respectively. Also, the effects of various parameters, such as initial concentration of RhB (5, 15, 25, and 35 mg L^{-1}), sonocatalyst amount (0, 0.25, 0.5, and 0.75 g L^{-1}), and concentration of H_2O_2 (0, 10, 20, 30, 40, 50, 60, and 70 mmol L^{-1}), on the sonocatalytic activity of MIL-101(Cr)/$CoFe_2O_4$ were investigated. The percentage degradation efficiency (DE%) was also determined using eqn (1) as follows:

$$DE\% = [(C_0 - C_t)/C_0] \times 100\% \quad (1)$$

where, C_0 and C_t represent the concentration (mg L^{-1}) of decomposed dye at the initial concentration (after adsorption equilibrium) and the specified reaction time interval in min, respectively.

3. Results and discussion

3.1. Characterization of the MIL-101(Cr)/$CoFe_2O_4$ nanocomposite

Fig. 1 demonstrates the X-ray diffraction (XRD) patterns of $CoFe_2O_4$, MIL-101(Cr) and MIL-101(Cr)/$CoFe_2O_4$ to characterize their phase and crystallization properties. As shown in Fig. 1(a), the main peaks identified for raw $CoFe_2O_4$ were located at 2θ values of 30.13°, 35.5°, 43.08°, 53.44°, 57.07° and 62.59°, which crystallized in the cubic structure with JCPDS card (01-1121). The average crystalline size of the $CoFe_2O_4$ nanoparticles was measured to around 12 nm utilizing the Scherrer equation.[30] The XRD pattern of MIL-101(Cr) is shown in Fig. 1(b). The diffraction peaks corresponding to reflection planes are indexed, which are consistent with the peak positions reported for the standard MIL-101(Cr) structure, demonstrating that the synthesized material has the MIL-101(Cr) phase with high crystallinity.[2] The XRD pattern of the nanocomposite in Fig. 1(c) exhibits diffraction peaks corresponding to both cubic structure $CoFe_2O_4$ and MIL-101(Cr), and no other impurity peaks can be observed. These results reveal that the sample is composed of spinel $CoFe_2O_4$ and MIL-101(Cr), and the MIL-101(Cr)/$CoFe_2O_4$ nanocomposite was successfully synthesized.

The Fourier transform infrared spectra (FTIR) of the as-prepared catalysts, namely $CoFe_2O_4$, MIL-101(Cr) and MIL-

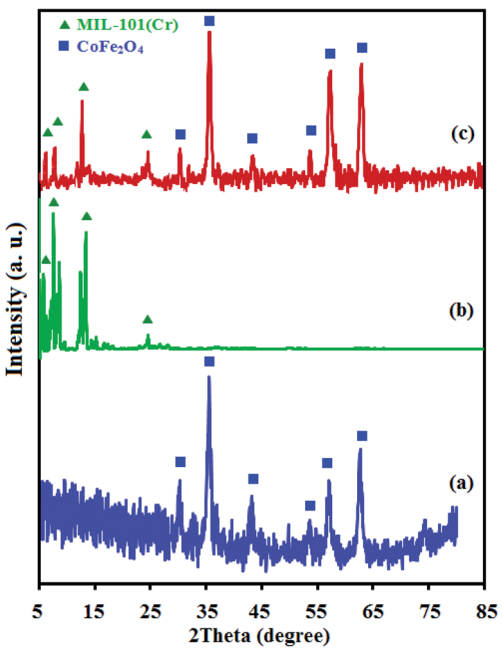

Fig. 1 XRD patterns of the as-fabricated (a) raw $CoFe_2O_4$, (b) raw MIL-101(Cr) and (c) MIL-101(Cr)/$CoFe_2O_4$.

101(Cr)/$CoFe_2O_4$, are displayed in Fig. 2. Fig. 2(a) shows the FT-IR spectrum of the $CoFe_2O_4$ nanoparticles with two peaks in the range of 400 to 600 cm^{-1}, corresponding to the Fe(III)–O and Co(II)–O bonds of spinel-type oxide.[31] In addition, the –OH group of adsorbed water resulted in the appearance of bands at about 2800–3700 cm^{-1} and 1400–1700 cm^{-1} related to the typical stretching vibrations.[32] As shown in Fig. 2(b), the characteristic absorption peaks of MIL-101(Cr) can be observed the region of 1400 to 1600 cm^{-1}, which mainly originate from the carboxylate group vibrations and are identical to that reported in the literature.[2] The two sharp peaks at 1600 and 1404 cm^{-1} can be attributed to the asymmetric and symmetric vibrations of the carboxyl groups, respectively, confirming the presence of the dicarboxylate linker inside the sample. After the formation of the MIL-101(Cr)/$CoFe_2O_4$ nanocomposite, as exhibited Fig. 2(c), the characteristic peaks related to MIL-101(Cr) are nearly the same and another band at 590 cm^{-1} is assigned to $CoFe_2O_4$. Combined, these results confirm the successful synthesis of the MIL-101(Cr)/$CoFe_2O_4$ nanocomposite.

Energy Dispersive X-ray (EDX) was performed to characterize the composition of the as-prepared nanocomposite. The chemical purity of the raw $CoFe_2O_4$ (Fig. S1(a)†) and raw MIL-101(Cr) (Fig. S1(b)†) was confirmed by EDX analysis. As shown in Fig. S1(c),† the EDX elemental spectrum of the nanocomposite shows elemental peaks corresponding to both MIL-101(Cr) (C, O and Cr) and $CoFe_2O_4$ (Co, Fe and O), and no other impurity peaks can be observed, demonstrating that the composite sample is composed of MIL-101(Cr) and $CoFe_2O_4$. The distribution of elements in the nanocomposite was examined utilizing SEM mapping analysis, and the results are shown in Fig. S1(d).† The corresponding elemental mappings show that Co, Fe, C, O and Cr elements are consistently distributed over the nanocomposite, confirming the homogeneity of the sample.

To survey the structure, morphology and size of the as-prepared samples, field emission scanning electron microscopy (FE-SEM) analysis was employed. The FE-SEM images of the raw $CoFe_2O_4$, raw MIL-101(Cr) and MIL-101(Cr)/$CoFe_2O_4$ nanocomposite are shown in Fig. 3. According to Fig. 3(a), the obtained $CoFe_2O_4$ nanoparticles are loosely aggregated with a sphere-like morphology. Moreover, it can be seen in Fig. 3(b) that the raw MIL-101(Cr) has an octahedral shape with crystals sizes in the submicrometer range (0.2–0.7 μm). Based on the SEM images of MIL-101(Cr)/$CoFe_2O_4$ (Fig. 3(c) and (d)), the different morphology of the binary MIL-101(Cr)/$CoFe_2O_4$ sample compared to that of the raw MIL-101 (Cr) indicates a different formation mechanism due to the presence of $CoFe_2O_4$ nanoparticles. However, although there was a change in morphology, the XRD, FT-IR, and EDX results strongly confirm that the MIL-101 (Cr) framework was present in the structure of as-synthesized nanocomposite.

The morphology and microstructure of the as-prepared MIL-101(Cr)/$CoFe_2O_4$ nanocomposite were further confirmed by TEM analysis. Fig. 4 presents the TEM images of the MIL-101(Cr)/$CoFe_2O_4$ nanocomposite. It is clear that the MIL-101(Cr) crystals and $CoFe_2O_4$ nanoparticles are both present in the composite. The nanoparticle size distribution is narrow, ranging from 15 to 40 nm. These results are consistent with the average particle size calculated in the XRD and FE-SEM analysis and are interesting and significant.

The UV-visible absorption spectra of $CoFe_2O_4$ and MIL-101(Cr)/$CoFe_2O_4$ nanocomposite are presented in Fig. S2.† As can be seen in Fig. S2(a),† the raw $CoFe_2O_4$ shows a broad absorption band with absorption edges at *ca.* 520 nm.[31] Compared with the spectrum of the raw $CoFe_2O_4$ sample, the spectral features of the MIL-101(Cr)/$CoFe_2O_4$ nanocomposite are shifted to the visible light region (Fig. S2(b)).† Additionally, the much stronger absorption band of MIL-101(Cr)/$CoFe_2O_4$ than that of raw $CoFe_2O_4$ indicates that the MIL-101(Cr)/$CoFe_2O_4$ nanocomposite has potential as an efficient sonocatalyst under visible light irradiation.

To precisely reveal the extraordinary structure of the as-prepared catalyst, BET analysis was performed. Fig. 5(a) and (c) show the nitrogen adsorption–desorption isotherms and the corresponding pore size distribution curves for MIL-101(Cr) and MIL-101(Cr)/$CoFe_2O_4$, respectively. The N_2 adsorption–desorption isotherms of the MIL-101(Cr)/$CoFe_2O_4$ nanocomposite in Fig. 5(c) demonstrate a type (IV) curve with H3 hysteresis loop. The BET specific surface area values for the raw MIL-101(Cr) and MIL-101(Cr)/$CoFe_2O_4$ were measured to be around 2452 and 3353 $m^2\ g^{-1}$ with the total pore volume of 0.532 and 3.0515 $cm^3\ g^{-1}$, respectively. Also, the pore sizes of the raw MIL-101(Cr) and MIL-101(Cr)/$CoFe_2O_4$ are 1.30 and 1.21 nm, which were computed utilizing the Barrett–Joyner–Halenda (BJH) method from the adsorption and desorption branches of the N_2 isotherms (Fig. 5(b) and (d)), respectively. Thus, based on these results, it can be concluded that adding $CoFe_2O_4$ during the synthesis process had a great effect on the structure and size of MIL-101(Cr) in the nanocomposite rather than the microstructure of pure MIL-101(Cr). Also confirming the above, the SEM images show that the size of MIL-101(Cr) in the MIL-101(Cr)/$CoFe_2O_4$ nanocomposite is in the nano-scale rather than that on the micro-scale of pure MIL-101(Cr), resulting in a significant increase in the pore volume and surface area of the nanocomposite, which can enhance the available active sites for its sonocatalytic performance.

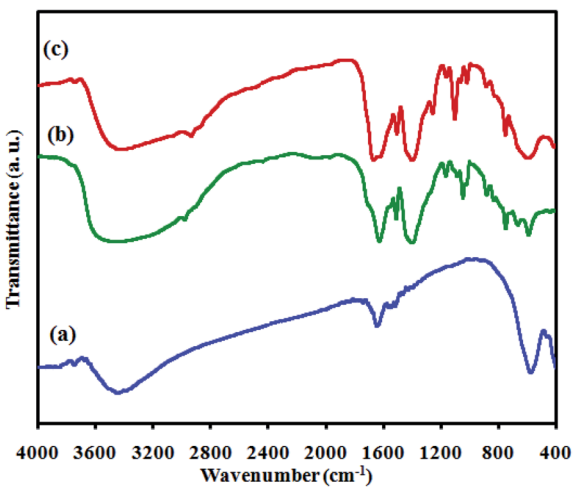

Fig. 2 FT-IR spectra of the as-fabricated (a) raw $CoFe_2O_4$, (b) raw MIL-101(Cr) and (c) MIL-101(Cr)/$CoFe_2O_4$.

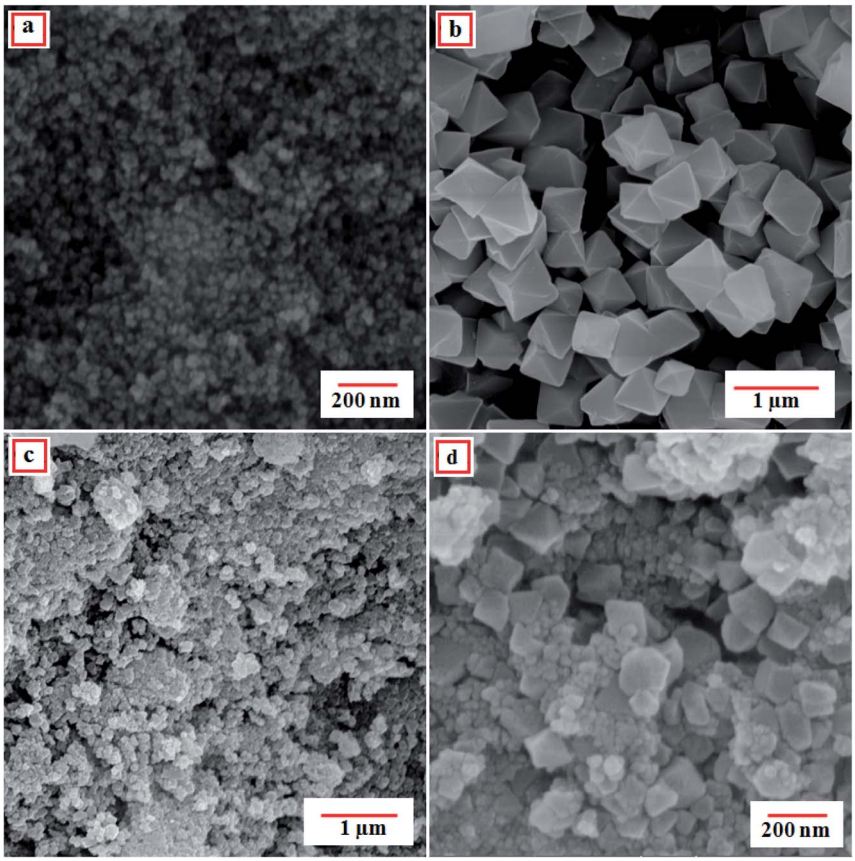

Fig. 3 FE-SEM images of the as-fabricated (a) $CoFe_2O_4$, (b) MIL-101(Cr) and (c and d) MIL-101(Cr)/$CoFe_2O_4$ nanocomposite.

Fig. S3† shows the magnetic hysteresis loops of the raw $CoFe_2O_4$ and MIL-101(Cr)/$CoFe_2O_4$, which were studied at room temperature with an applied field of $-10\,000 \leq H \leq 10\,000$ Oe. As shown in Fig. S3,† the ferromagnetic properties of both $CoFe_2O_4$ and MIL-101(Cr)/$CoFe_2O_4$ were obviously confirmed. As anticipated, the MIL-101(Cr)/$CoFe_2O_4$ nanocomposite had a lower saturation magnetization (Ms) (22 emu g^{-1}) than that of the raw $CoFe_2O_4$ (62.78 emu g^{-1}) due to the presence of the nonmagnetic MIL-101(Cr). However, compared with the non-magnetic MIL-101(Cr) catalyst, the magnetic MIL-101(Cr)/$CoFe_2O_4$ catalyst could be separated from the heterogeneous reaction system using an external magnetic field, as shown in the inset of Fig. S3.†

3.2. Sonocatalytic activity of MIL-101(Cr)/$CoFe_2O_4$ nanocomposite

The sonocatalytic performance of the MIL-101(Cr)/$CoFe_2O_4$ nanocomposite was investigated for the degradation of the

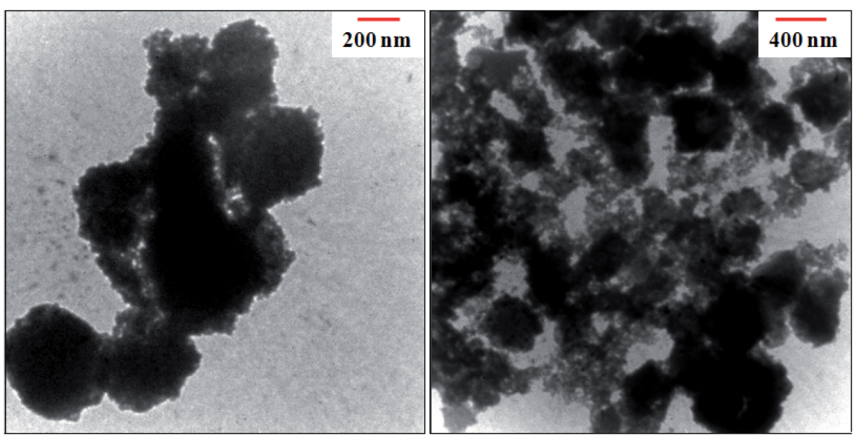

Fig. 4 TEM images of the as-fabricated MIL-101(Cr)/$CoFe_2O_4$ nanocomposite.

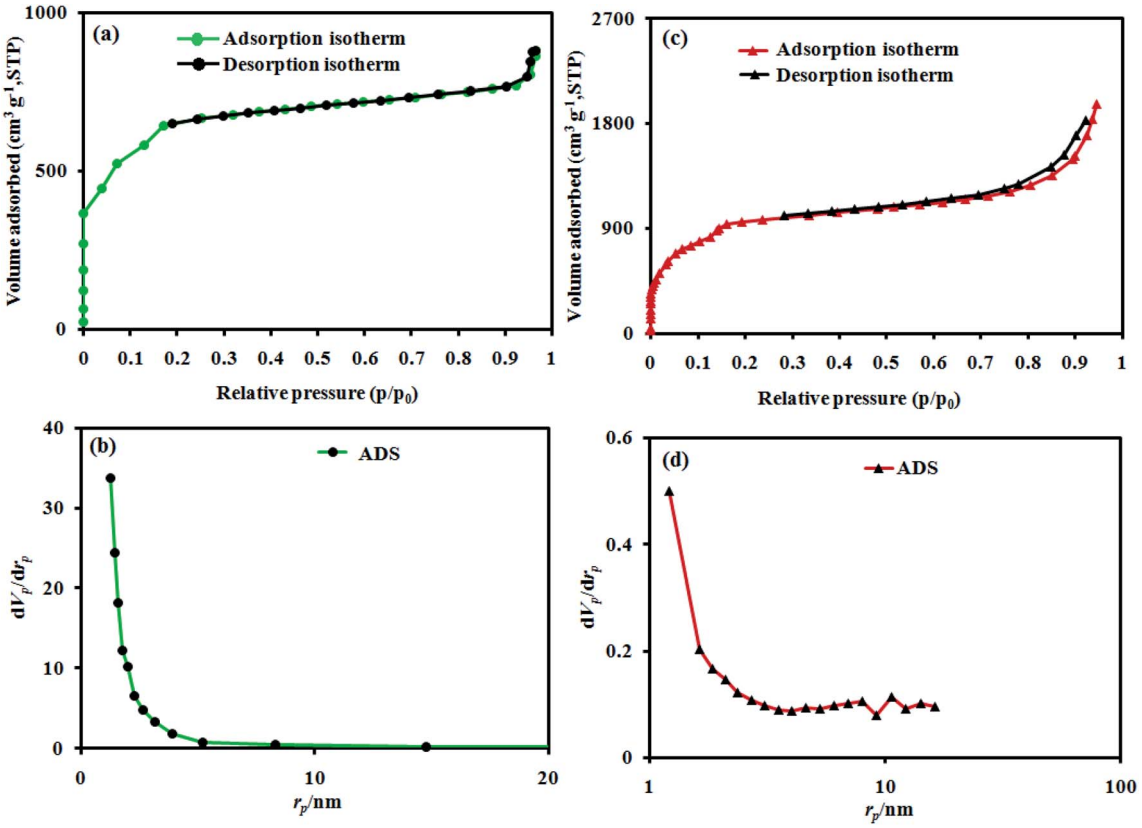

Fig. 5 BET analysis and BJH plots of the as-fabricated (a and b) raw MIL-101(Cr), and (c and d) MIL-101(Cr)/$CoFe_2O_4$.

cationic RhB dye and anionic MO dye under US irradiation. Fig. 6(a) shows the change in the UV-vis absorbance spectrum and color of RhB as a function of irradiation time. Firstly, the adsorption percentage of RhB by the MIL-101(Cr)/$CoFe_2O_4$ nanocomposite at 30 min in the dark under adsorption–desorption equilibrium was only 11%, which is related to the fact that the cationic charges on the MIL-101(Cr)/$CoFe_2O_4$ nanocomposite repel the cationic charged RhB dye molecules.[33] In the presence of the sonocatalyst, H_2O_2 and US irradiation, the intensity of the characteristic absorption peak of RhB at 557 nm diminished continuously with time and it roughly disappeared after 140 min. The sonocatalytic activity of the MIL-101(Cr)/$CoFe_2O_4$ nanocomposite for the degradation of the anionic MO dye was considered to confirm the generality of this sonocatalytic system. The adsorption percentage of MO by the MIL-101(Cr)/$CoFe_2O_4$ nanocomposite within 30 min of adsorption–desorption equilibrium was 39%, which can attributed to the adsorption of the anionic molecules of MO with the cationic charged nanocomposite. As shown in Fig. 6(b), the degradation efficiency was 88% for MO in the MIL-101(Cr)/$CoFe_2O_4$/H_2O_2/US system within 140 min. It was discovered that the as-prepared nanocomposite acted differently in the sonocatalytic degradation of the RhB and MO dyes due to their distinct structures, compositions, size and electric charge.[30]

To provide an overview on the potential and workability of each component in the decomposition reaction of RhB dye, several systems including US alone, H_2O_2/US, MIL-101(Cr)/$CoFe_2O_4$/H_2O_2, MIL-101(Cr)/H_2O_2/US, MIL-101(Cr)/$CoFe_2O_4$/US, $CoFe_2O_4$/H_2O_2/US, and MIL-101(Cr)/$CoFe_2O_4$/H_2O_2/US were utilized for the degradation of the dyes and the results are presented in Fig. 6(c). Briefly, the results from the executed tests revealed that decomposition efficiency followed the order of US alone (0%) < H_2O_2/US (12%) < MIL-101(Cr)/$CoFe_2O_4$/H_2O_2 ~ MIL-101(Cr)/H_2O_2/US (25%) < MIL-101(Cr)/$CoFe_2O_4$/US (31%) < $CoFe_2O_4$/H_2O_2/US (52%) < MIL-101(Cr)/$CoFe_2O_4$/H_2O_2/US (96%). According to the analysis of the results, MIL-101(Cr)/$CoFe_2O_4$/H_2O_2/US was recognized as the best system for the decomposition of RhB, which can be related to the obstruction of electron–hole recombination by the linkage between $CoFe_2O_4$ and MIL-101(Cr).

The kinetics of the RhB dye degradation was investigated using the rate constant (k) for a much better comparison of the sonocatalytic efficiency of the samples. Therefore, to assess the rate of the reaction in the sonodegradation experiments, the pseudo-first-order equation was used[1] as follows: $\ln(C_0/C) = kt$, where C_0 and C are the dye concentrations before and after irradiation, respectively, k is the pseudo-first-order rate constant and t is the reaction time. As shown in Fig. 6(d), the rate constant, k, in the different systems increased in the order of US alone (0 min^{-1}) < H_2O_2/US (0.0009 min^{-1}) < MIL-101(Cr)/$CoFe_2O_4$/H_2O_2 ~ MIL-101(Cr)/H_2O_2/US (0.0018 min^{-1}) < MIL-101(Cr)/$CoFe_2O_4$/US (0.0026 min^{-1}) < $CoFe_2O_4$/H_2O_2/US (0.0055 min^{-1}) < MIL-101(Cr)/$CoFe_2O_4$/H_2O_2/US (0.0215 min^{-1}). Among them, the MIL-101(Cr)/$CoFe_2O_4$/H_2O_2/US system

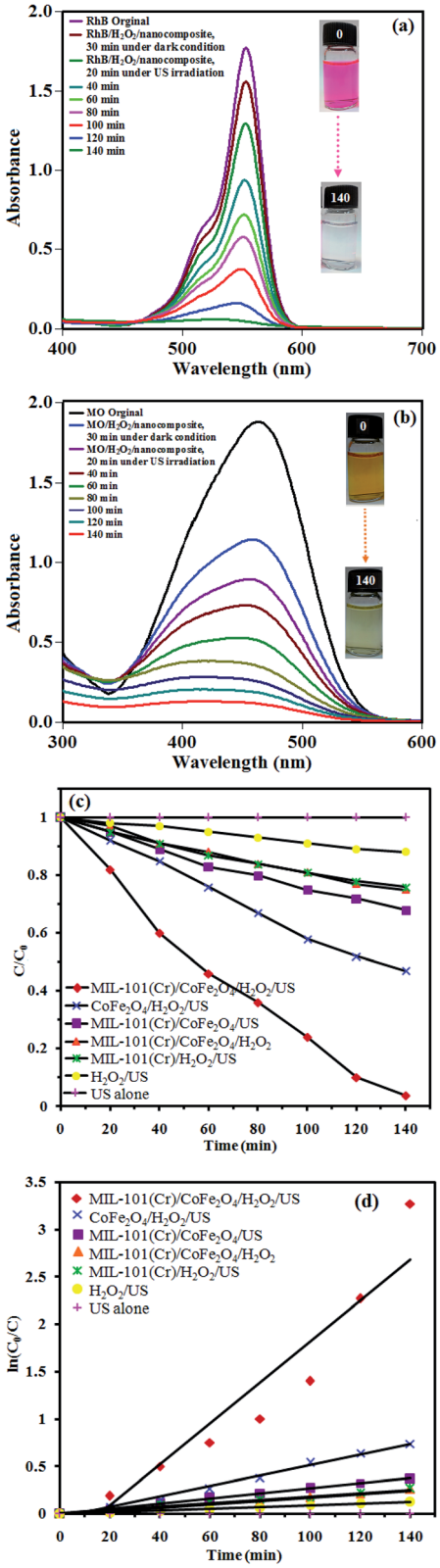

Fig. 6 UV-vis absorption spectra of the sonodegradation process of (a) RhB and (b) MO dye over the MIL-101(Cr)/$CoFe_2O_4$ nanocomposite as a function of irradiation time, (c) sonocatalytic degradation of RhB and (d) plot of $\ln(C_0/C)$ against the irradiation time under different conditions. (Experimental conditions: catalyst dosage = 0.5 g L^{-1}, RhB dye = 25 mg L^{-1} (50 mL), pH = 7 (about 6.5), H_2O_2 = 60 mmol L^{-1}, temperature = 25 °C and reaction time = 140 min.)

exhibited the best catalytic performance (96% within 140) with a rate constant of 0.0215 min^{-1}, which was enhanced by more than 12 and 4 times (k = 0.0215 min^{-1}) compared to that of the raw MIL-101(Cr) (k = 0.0018 min^{-1}) and $CoFe_2O_4$ (k = 0.0055 min^{-1}), respectively. The raw MIL-101(Cr) and $CoFe_2O_4$ showed poor sonocatalytic activities of only 25% and 52% degradation of RhB within 140 min of US, respectively, which resulted from the quick recombination of photoexcited charges. Thus, when MIL-101(Cr) was composited with $CoFe_2O_4$ nanoparticles, then the sonodegradation rate increased prominently.

3.2.1. Effect of H_2O_2 amount, sonocatalyst dosage and initial concentration of RhB. To explore the influence of H_2O_2 concentration on the degradation of RhB, a series of tests were applied with different amounts of H_2O_2, while the initial concentration of dye and other parameters were kept constant, and the results are displayed in Fig. S4(a).† It can be seen that only 31% of RhB was removed without H_2O_2. When the concentration of H_2O_2 increased from 10 to 60 mmol L^{-1}, the degradation efficiency was enhanced correspondingly from 38% to 96%. This improvement in the degradation rate can be attributed to the increase in hydroxyl radicals (·OH) produced *via* H_2O_2 decomposition. However, the further addition of H_2O_2 to 70 mmol L^{-1} led to a decline in the degradation proficiency. Therefore, excess H_2O_2 molecules act as scavengers of ·OH to create perhydroxyl (·OOH) radicals with a lower oxidation potential.[1]

To optimize the effect of sonocatalyst dosage on the degradation process of RhB dye, a series of experiments was performed with different concentrations of MIL-101(Cr)/$CoFe_2O_4$ nanocomposite (0, 0.25, 0.5 and 0.75 g L^{-1}, Fig. S4(b)),† while the other parameters were kept constant. Apparently, with an increase in the catalyst concentration from 0 to 0.5 g L^{-1}, an increase in the degradation rate of RhB in aqueous solution occurred (from 12% to 96%), which is reasonable due to the increase in the number of active sites resulting from a higher amount of catalyst. Clearly, it generated more ·OH radicals, facilitating the further and faster degradation of the dye molecules.[34] However, a higher concentration of MIL-101(Cr)/$CoFe_2O_4$ (0.5 to 0.75 g L^{-1}) lead to a decline in the degradation efficiency because of the aggregation of the nanoparticles and decrease in the number of active sites, as well as the scattering and blockage of the transmission of ultrasound waves within the solution. Subsequently, the optimal value of 0.5 g L^{-1} for MIL-101(Cr)/$CoFe_2O_4$ was considered for the other tests.[35]

The effect of initial dye concentration as a critical parameter on its sonocatalytic degradation efficiency was investigated. Accordingly, different initial concentrations of RhB ranging from 5 to 35 mg L^{-1} were tested under US irradiation. As shown in Fig. S4(c),† more time was required to achieve a reasonable degradation efficiency at a higher concentration of RhB dye. However, the number of generated ·OH radicals required for attacking the dye molecules remained constant at a constant reaction time, amount of H_2O_2 and catalyst dosage, and increasing the initial dye concentration resulted in a decrease in the degradation efficiency.[3]

The pH of the initial solution is a significant parameter that affects the degradation of dye molecules. The influence of the

initial pH of the RhB and MO dye solutions on their sonocatalytic degradation is shown in Fig. S4(d).† To explore the effect of pH on the degradation efficiency, the pH of the dye solutions was adjusted over a wide range, ranging from acidic, neutral/near-neutral to basic. For these trial runs, the dose of the catalyst was 0.5 g L^{-1}, the initial dye concentration was set to 25 mg L^{-1} (50 mL), and the amount of H_2O_2 was 60 mmol L^{-1}. Approximately 51%, 91%, 96%, 100% and 53% of RhB and 44%, 95%, 88%, 80% and 40% of MO was degraded after 140 min of reaction at the initial pH 3, 5, 7, 9 and 11, respectively. Based on the results of the effect of initial pH on the degradation of the dyes, the degradation efficiency reached the highest level when the initial RhB and MO solutions had a neutral pH. Thus, the acceptable performance of MIL-101(Cr)/$CoFe_2O_4$ as an efficient heterogeneous catalyst in a tunable neutral solution of organic dyes are a noteworthy advantage for increasing its efficiency and reducing the cost of the process. This may be related to the function of the solid-acid catalyst of MIL-101(Cr), which will be introduced in detail below. On the other hand, the degradation dramatically decreased at pH 3 and 11, which is reasonable because MOFs suffer from a lack of stability in alkaline and acidic conditions compared to a neutral environment, hindering the catalytic process.[36]

3.2.2. The proposed sonocatalytic degradation mechanism of organic dye. The sonocatalytic degradation of organic contaminants over a sonocatalyst is based on both sonoluminescence and hot spots, which originate from the ultrasonic-cavitation effect.[24,25] Sonoluminescence seems can produce abundant visible light, which excites the prepared MIL-101(Cr)/$CoFe_2O_4$ nanocomposite, and subsequently it acts as a sonocatalyst. Moreover, the formation of hot spots results in the generation of electrons and holes on the surface of the MIL-101(Cr)/$CoFe_2O_4$ sonocatalyst.[17,31,37] Actually, the electrons in the full valence band of MIL-101(Cr) and $CoFe_2O_4$ are excited to the empty conduction band separately under ultrasound irradiation, leaving an equal number of holes with a positive charge in the corresponding positions. The presence of $CoFe_2O_4$ favors the sonocatalytic activity under ultrasound irradiation due to its narrow band gap. Moreover, the difference in the band structures of $CoFe_2O_4$ and MIL-101(Cr) facilitates the transfer of sono-induced electrons from the CB of $CoFe_2O_4$ to the CB of MIL-101(Cr) and holes migrate from the VB of MIL-101(Cr) to the VB of $CoFe_2O_4$. These processes productively prevent the recombination of sonogenerated electron–hole pairs and significantly improve the sonocatalytic activity. The sono-excited electrons on the surface of MIL-101(Cr) may be captured by H_2O_2 and O_2 in the solution to yield ·OH and $O_2^{\cdot-}$ radicals, while the holes are scavenged by the adsorbed water to form ·OH radicals. Finally these active species can oxidize the dye molecules adsorbed on the active sites of MIL-101(Cr) and $CoFe_2O_4$ through electrostatic attraction, resulting in the degradation of the dye and production of CO_2, H_2O, *etc.* as safe materials[17,30,31,38,39] (eqn (2)–(9)). Thus, based on this process, a schematic representation of the mechanism is illustrated in Fig. 7.

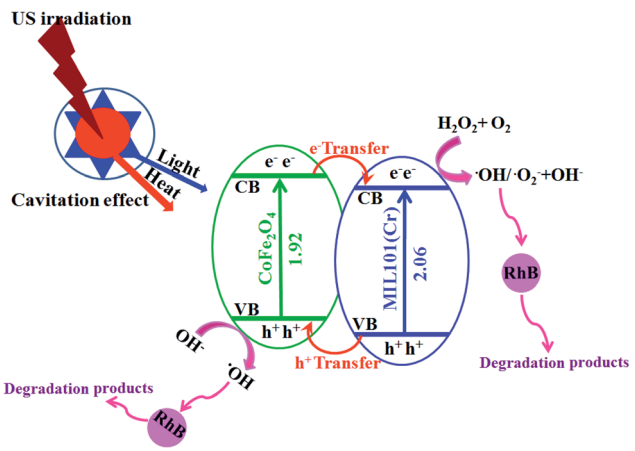

Fig. 7 Conceivable mechanism for the sonodegradation process of dye contaminants using the MIL-101(Cr)/$CoFe_2O_4$/H_2O_2/US system in aqueous solution.

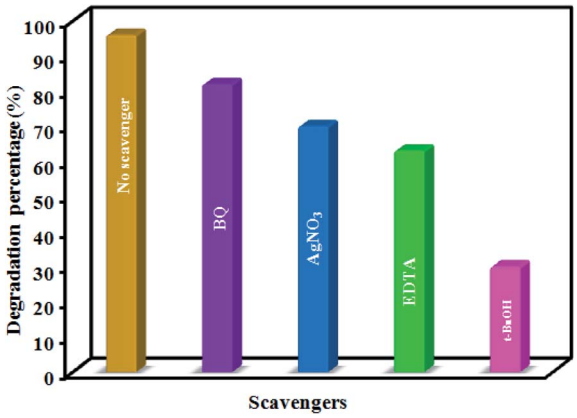

Fig. 8 Effects of different scavengers on the sonocatalytic degradation of RhB in the MIL-101(Cr)/$CoFe_2O_4$/H_2O_2/US system. (Experimental conditions: scavenger = 10 mmol L^{-1}, catalyst dosage = 0.5 g L^{-1}, RhB dye = 25 mg L^{-1} (50 mL), pH = 7 (about 6.5), H_2O_2 = 60 mmol L^{-1}, temperature = 25 °C and reaction time = 140 min.)

$$\text{US irradiation} \rightarrow \text{heat–light} \quad (2)$$

$$\text{MIL-101(Cr)/CoFe}_2\text{O}_4 + \text{heat or light} \rightarrow (\text{MIL-101(Cr)/CoFe}_2\text{O}_4)^* \quad (3)$$

$$(\text{CoFe}_2\text{O}_4)^* \rightarrow \text{CoFe}_2\text{O}_4\ (h_{VB}^+) + \text{CoFe}_2\text{O}_4\ (e_{CB}^-) \quad (4)$$

$$(\text{MIL-101(Cr)})^* \rightarrow \text{MIL-101(Cr)}\ (h_{VB}^+) + \text{MIL-101(Cr)}\ (e_{CB}^-) \quad (5)$$

$$\text{CoFe}_2\text{O}_4\ (e_{CB}^-) + \text{MIL-101(Cr)} \rightarrow \text{CoFe}_2\text{O}_4 + \text{MIL-101(Cr)}\ (e_{CB}^-) \quad (6)$$

$$\text{MIL-101(Cr)}\ (e_{CB}^-) + H_2O_2 \text{ and } O_2 \rightarrow \text{MIL-101(Cr)} + OH^- + \cdot OH \text{ and } O_2^{\cdot-} \quad (7)$$

$$\text{CoFe}_2\text{O}_4\ (h_{VB}^+) + H_2O/OH^- \rightarrow \text{CoFe}_2\text{O}_4 + \cdot OH \quad (8)$$

$$\text{RhB} + \cdot OH \text{ and } O_2^{\cdot-} \rightarrow CO_2 + H_2O + \textit{etc.} \quad (9)$$

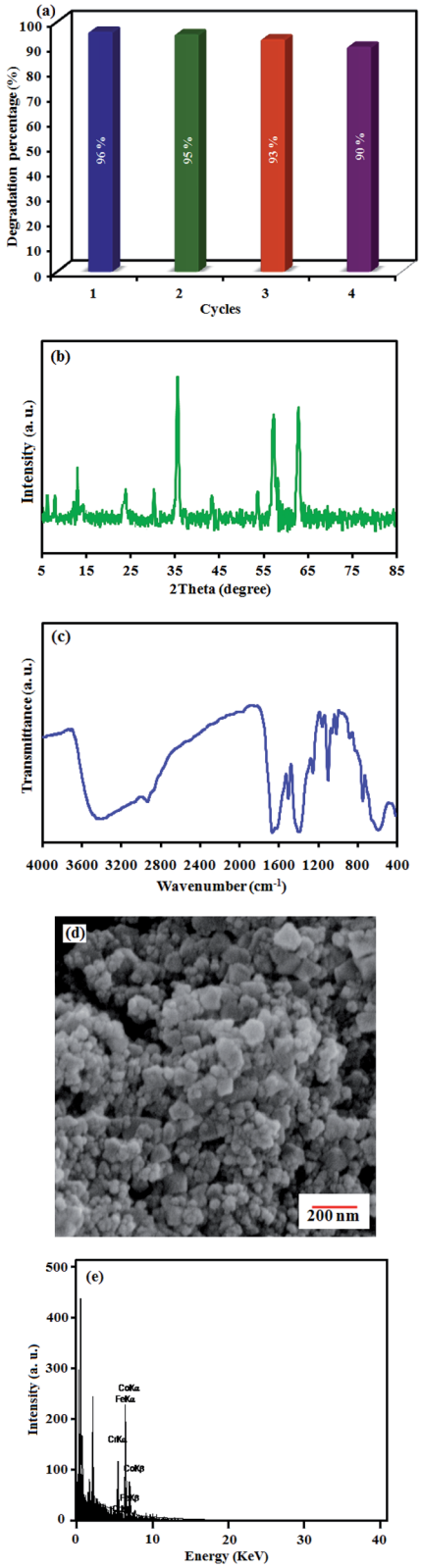

Fig. 9 (a) Recyclability of MIL-101(Cr)/$CoFe_2O_4$ nanocomposite. (b) XRD, (c) FT-IR, (d) FE-SEM and (e) EDX results of MIL-101(Cr)/$CoFe_2O_4$ recovered after the fourth run.

3.2.3. The influence of the scavenger type. To investigate what type of species plays a crucial role in the sonodecomposition process of the dyes and confirm the mechanism of sonocatalysis, disodium ethylenediaminetetraacetate (EDTA), $AgNO_3$, 1,4-benzoquinone (BQ) and *t*-butyl alcohol (*t*-BuOH) were used as the scavengers of holes (h_{VB}^+), electrons, $O_2^{\bullet-}$ and ·OH radicals, respectively, with the same initial concentration of 10 mmol L^{-1}. As shown in Fig. 8, RhB sonodecomposition using the MIL-101(Cr)/$CoFe_2O_4$ nanocomposite was significantly suppressed after the addition of *t*-BuOH, demonstrating that ·OH is the most reactive species in the sonocatalytic process. When $AgNO_3$, BQ, and EDTA were added, the sonodecomposition activity of the MIL-101(Cr)/$CoFe_2O_4$ nanocomposite slightly diminished, which shows that electrons, $O_2^{\bullet-}$ and h^+ play a minor role. Thus, the most reactive species involved in the decomposition of RhB over the MIL-101(Cr)/$CoFe_2O_4$ nanocomposite are ·OH radicals, while electrons, $O_2^{\bullet-}$ and h^+ are also generated during the sonocatalytic reaction under ultrasound irradiation.[40,41]

3.2.4. Comparison with other reported sonocatalysts. To show the benefit of the present degradation strategy, the obtained results from sonodegradation of RhB over the MIL-101(Cr)/$CoFe_2O_4$ nanocomposite were compared with some reported catalysts in the literature.[3,18,42–50] The comparison between the results in this study with the catalysts in the literature in shown in Table S1† based on different parameters including initial dye concentration, degradation time, consumed catalyst amount and percentage, which illustrates the excellent degradation efficiency of the MIL-101(Cr)/$CoFe_2O_4$ nanocomposite. Especially, the degradation reaction in the presence of most detailed catalysts took longer times and required a higher catalyst to dye ratio.

3.2.5. Recyclability and stability tests. One of the most interesting advantages with the use of heterogeneous catalysts in wastewater treatment is their potential for reuse over several runs. Thus, the reusability of the sonocatalyst was investigated after its magnetic separation, washing completely with water and ethanol and then assessment of sonocatalysis for four cycles (Fig. 9(a)). The results showed that the degradation efficiency only diminished slightly even after four times of reuse, demonstrating that the MIL-101(Cr)/$CoFe_2O_4$ sonocatalyst has a great stability. The amounts of Cr, Co and Fe metals in the filtrate were also determined to be approximately 0.1% by ICP-AES investigation. This data proves that the leaching of Co^{2+}, Cr^{3+} and Fe^{3+} ions from the catalyst was not significant. The nature of the recovered catalyst was also tested. As shown in Fig. 9(b)–(e), the XRD, FT-IR, FE-SEM and EDX analyses of the recycled MIL-101(Cr)/$CoFe_2O_4$ catalyst showed no change compared with that of the fresh sample. These findings confirm that the structure of the MIL-101(Cr)/$CoFe_2O_4$ nanocomposite is stable under the reaction conditions as a special advantage for its practical application.

4. Conclusion

In summary, a new binary magnetic MIL-101(Cr)/$CoFe_2O_4$ sonocatalyst for the degradation of dyes was fabricated *via*

a hydrothermal method and completely characterized using various techniques including XRD, FT-IR, FE-SEM, EDX, TEM, UV-vis, BET and VSM. The results revealed that the as-prepared nanocomposite had good sonocatalytic activity toward the degradation of RhB (in the presence of H_2O_2 as an ·OH source) particularly compared to its individual counterparts. The performance of the sonocatalyst was additionally proven to be dependent on the amount of applied H_2O_2, initial dye concentration and the catalyst dosage. Additionally, the excellent superparamagnetism at room temperature and stability of the MIL-101(Cr)/$CoFe_2O_4$ nanocomposite guarantee its applicable magnetic separation. The high sonocatalytic performance of MIL-101(Cr)/$CoFe_2O_4$ was attributed to the combination of the adsorption and catalytic properties of MIL-101(Cr) and magnetic properties of $CoFe_2O_4$ together with the efficient separation of electron–hole pairs, making it a successful and efficient sonocatalyst for environmental applications.

Conflicts of interest

There are no conflicts to declare.

Acknowledgements

The authors sincerely acknowledge all supports from Dr Firouzeh Siadatnasab for her scientific and laboratory assistance at Lorestan University.

References

1 S. Farhadi and F. Siadatnasab, *Mater. Res. Bull.*, 2016, **83**, 345–353.
2 A. A. Hoseini, S. Farhadi and A. Zabardasti, *Appl. Organomet. Chem.*, 2019, **33**, e4656.
3 S. Farhadi and F. Siadatnasab, *Desalin. Water Treat.*, 2017, **66**, 299–308.
4 C. H. Nguyen and R.-S. Juang, *J. Ind. Eng. Chem.*, 2019, **76**, 296–309.
5 S. Farhadi, M. Dusek, F. Siadatnasab and V. Eigner, *Polyhedron*, 2017, **126**, 227–238.
6 E. Ferrer-Polonio, B. Pérez-Uz, J. A. Mendoza-Roca, A. Iborra-Clar and L. Pastor-Alcañiz, *J. Ind. Eng. Chem.*, 2017, **56**, 364–374.
7 Y. Wang, L. Zhu, X. Wang, W. Zheng, C. Hao, C. Jiang and J. Wu, *J. Ind. Eng. Chem.*, 2018, **61**, 321–330.
8 S. H. Yoo, S.-I. Lee, H.-I. Joh and S. Lee, *J. Ind. Eng. Chem.*, 2018, **63**, 27–32.
9 J. Xu, P. Xin, Y. Gao, B. Hong, H. Jin, D. Jin, X. Peng, J. Li, J. Gong and H. Ge, *Mater. Chem. Phys.*, 2014, **147**, 915–919.
10 W. Qiu, D. Yang, J. Xu, B. Hong, H. Jin, D. Jin, X. Peng, J. Li, H. Ge and X. Wang, *J. Alloys Compd.*, 2016, **678**, 179–184.
11 H. Chen, Y. Yang, J. Wei, J. Xu, J. Li, P. Wang, J. Xu, Y. Han, H. Jin and D. Jin, *Mater. Sci. Eng., B*, 2019, **249**, 114420.
12 P. Saharan, G. R. Chaudhary, S. Lata, S. Mehta and S. Mor, *Ultrason. Sonochem.*, 2015, **22**, 317–325.
13 Y. L. Pang and A. Z. Abdullah, *Ultrason. Sonochem.*, 2012, **19**, 642–651.
14 S. Zhang, *Ultrason. Sonochem.*, 2012, **19**, 767–771.
15 Y. Wang, L. Gai, W. Ma, H. Jiang, X. Peng and L. Zhao, *Ind. Eng. Chem. Res.*, 2015, **54**, 2279–2289.
16 R. D. C. Soltani, S. Jorfi, H. Ramezani and S. Purfadakari, *Ultrason. Sonochem.*, 2016, **28**, 69–78.
17 H. Zhang, C. Wei, Y. Huang and J. Wang, *Ultrason. Sonochem.*, 2016, **30**, 61–69.
18 M. Zhou, H. Yang, T. Xian, R. Li, H. Zhang and X. Wang, *J. Hazard. Mater.*, 2015, **289**, 149–157.
19 Y. Areerob, J. Y. Cho, W. K. Jang and W.-C. Oh, *Ultrason. Sonochem.*, 2018, **41**, 267–278.
20 A. Khataee, S. Saadi and B. Vahid, *Ultrason. Sonochem.*, 2017, **34**, 98–106.
21 H. Deng, X. Li, Q. Peng, X. Wang, J. Chen and Y. Li, *Angew. Chem.*, 2005, **117**, 2842–2845.
22 Y. Fu, Q. Chen, M. He, Y. Wan, X. Sun, H. Xia and X. Wang, *Ind. Eng. Chem. Res.*, 2012, **51**, 11700–11709.
23 G. Zhang, J. Qu, H. Liu, A. T. Cooper and R. Wu, *Chemosphere*, 2007, **68**, 1058–1066.
24 X.-J. Dui, X.-Y. Wu, J.-Z. Liao, T. Teng, W.-M. Wu and W.-B. Yang, *Inorg. Chem. Commun.*, 2015, **56**, 112–115.
25 D. Meziani, K. Abdmeziem, S. Bouacida, M. Trari and H. Merazig, *Sol. Energy Mater. Sol. Cells*, 2016, **147**, 46–52.
26 V. M. Correia, T. Stephenson and S. J. Judd, *Environ. Technol.*, 1994, **15**, 917–929.
27 P. Mahata, G. Madras and S. Natarajan, *J. Phys. Chem. B*, 2006, **110**, 13759–13768.
28 P. Chowdhury, C. Bikkina and S. Gumma, *J. Phys. Chem. C*, 2009, **113**, 6616–6621.
29 P. Horcajada, C. Serre, M. Vallet-Regí, M. Sebban, F. Taulelle and G. Férey, *Angew. Chem., Int. Ed.*, 2006, **45**, 5974–5978.
30 S. Farhadi, F. Siadatnasab and A. Khataee, *Ultrason. Sonochem.*, 2017, **37**, 298–309.
31 F. Siadatnasab, S. Farhadi and A. Khataee, *Ultrason. Sonochem.*, 2018, **44**, 359–367.
32 B. Senthilkumar, R. K. Selvan, P. Vinothbabu, I. Perelshtein and A. Gedanken, *Mater. Chem. Phys.*, 2011, **130**, 285–292.
33 T. Wang, P. Zhao, N. Lu, H. Chen, C. Zhang and X. Hou, *Chem. Eng. J.*, 2016, **295**, 403–413.
34 W. Luo, L. Zhu, N. Wang, H. Tang, M. Cao and Y. She, *Environ. Sci. Technol.*, 2010, **44**, 1786–1791.
35 F. Siadatnasab, S. Farhadi, M. Dusek, V. Eigner, A.-A. Hoseini and A. Khataee, *Ultrason. Sonochem.*, 2019, 104727.
36 C. Zhao, P. Dong, Z. Liu, G. Wu, S. Wang, Y. Wang and F. Liu, *RSC Adv.*, 2017, **7**, 24453–24461.
37 P. Qiu, W. Li, B. Thokchom, B. Park, M. Cui, D. Zhao and J. Khim, *J. Mater. Chem. A*, 2015, **3**, 6492–6500.
38 H. T. M. Thanh, N. T. T. Tu, N. P. Hung, T. N. Tuyen, T. X. Mau and D. Q. Khieu, *J. Porous Mater.*, 2019, **26**, 1699–1712.
39 M. Sadeghi, S. Farhadi and A. Zabardasti, *RSC Adv.*, 2020, **10**, 10082–10096.
40 J. Monteagudo, A. Durán and I. San Martín, *J. Environ. Manage.*, 2014, **141**, 61–69.
41 T. Xu, L. Zhang, H. Cheng and Y. Zhu, *Appl. Catal., B*, 2011, **101**, 382–387.

42 N. Wang, L. Zhu, M. Wang, D. Wang and H. Tang, *Ultrason. Sonochem.*, 2010, **17**, 78–83.
43 X. Chen, J. Dai, G. Shi, L. Li, G. Wang and H. Yang, *Ultrason. Sonochem.*, 2016, **29**, 172–177.
44 L. Zhu, S.-B. Jo, S. Ye, K. Ullah and W.-C. Oh, *Chin. J. Catal.*, 2014, **35**, 1825–1832.
45 G. Wang, Y. Huang, G. Li, H. Zhang, Y. Wang, B. Li, J. Wang and Y. Song, *Ultrason. Sonochem.*, 2017, **38**, 335–346.
46 L. Zhu, Z.-D. Meng, C.-Y. Park, T. Ghosh and W.-C. Oh, *Ultrason. Sonochem.*, 2013, **20**, 478–484.
47 M. Sadeghi, A. Zabardasti, S. Farhadi, S. Yekta and D. Mirzaei, *J. Water Process. Eng.*, 2019, **32**, 100946.
48 S. Kamal, G.-T. Pan, S. Chong and T. C.-K. Yang, *Processes*, 2020, **8**, 104.
49 E. Abroushan, S. Farhadi and A. Zabardasti, *RSC Adv.*, 2017, **7**, 18293–18304.
50 S. Bai, X. Shen, X. Zhong, Y. Liu, G. Zhu, X. Xu and K. Chen, *Carbon*, 2012, **50**, 2337–2346.